Investigation of CLYC-6 for thermal neutron detection and CLYC-7 for fast neutron spectrometry

Francesca Ferrulli, Marc Labalme, Marco Silari

Investigation of CLYC-6 for thermal neutron detection and CLYC-7 for fast neutron spectrometry

Francesca Ferrulli [(1,2,*)], Marc Labalme [(1)], Marco Silari [(2)]

[(1)] Laboratoire de Physique Corpusculaire de Caen, Normandie Université, ENSICAEN, UNICAEN, CNRS/IN2P3, 14000 Caen, France

[(2)] CERN, 1211 Geneva 23, Switzerland

Abstract

Highly enriched ^{6}Li and ^{7}Li Cs_2LiYCl_6 (CLYC) scintillators were investigated in view of their application as thermal neutron counter (CLYC-6) and as fast neutron spectrometer (CLYC-7) in the recently developed B-RAD radiation survey meter, an instrument designed to work in regions of high magnetic fields, currently equipped with a probe for photon dose rate measurements and γ-spectrometry. Both crystals were irradiated with a 2.5 MeV mono-energetic neutron beam from a Deuterium-Deuterium (D-D) generator and characterised in terms of neutron/γ-ray (n/γ) discrimination capability by the Pulse Shape Discrimination (PSD) method, energy resolution and quenching factor. Both crystals exhibit an excellent n/γ discrimination, quantified by a Figure of Merit higher than 2. The measured thermal energy resolution of CLYC-6 is 6%. The quenching factor for the ^{6}Li(n,t)α thermal neutron reaction is 0.65 and for the ^{35}Cl(n,p)^{35}S reaction is 0.91. The measured neutron detection efficiency per unit volume of CLYC-6 is 60% higher than that of a ^{3}He proportional counter. CLYC-7 was tested as a fast neutron spectrometer below 10 MeV, when irradiated with continuum neutron spectra from Am-Be and ^{252}Cf sources. A proton/α-particle (p/α) discrimination was performed exploiting the PSD technique, without any unfolding procedure. The resulting spectra match the corresponding ISO spectra better than the spectra without the p/α discrimination, especially in the range 3 MeV to 5 MeV. A more sensitive PSD algorithm might help to improve particle discrimination at lower energies, while different reaction channels arise at higher energies preventing a spectrometry analysis.

Keywords– *CLYC-6, CLYC-7, fast neutron spectrometry, thermal neutron counter, Pulse Shape Discrimination.*

1. Introduction

Cs_2LiYCl_6:Ce (CLYC) is a promising inorganic scintillator from the elpasolite family. It is characterised by high density (3.3 g cm^{-3}), high Z_{eff} (54), light yield linearity down to low energies (the light yield variation is 1.6% from 662 keV down to 14.4 keV) and good energy resolution (5% at 662 keV) [1]. It can detect both γ-ray and neutron radiation with excellent neutron/γ-ray (n/γ) discrimination capability by the Pulse Shape Discrimination (PSD) technique [2].

Two CLYC crystals were considered in this work, one enriched in ^{6}Li and one enriched in ^{7}Li. We will refer to them as CLYC-6 and CLYC-7 respectively. The former is suitable for thermal neutron detection via the ^{6}Li(n,t)α reaction [3]. The latter is commonly used for fast neutron measurements through the ^{35}Cl(n,p)^{35}S and ^{35}Cl(n,α)^{32}P reactions below ~8 MeV [4]. Between 8 MeV and 18 MeV, the cross section of the (n,p) and (n,α) reactions to the ground and excited states of ^{35}S and ^{32}P, respectively, are comparable and the different reactions cannot be distinguished [4]. Above ~ 20 MeV the cross sections of the (n,t) and (n,d) reactions become also comparable [5]. CLYC-7 was also recently investigated [6–8] as a fast neutron spectrometer without unfolding below about 10 MeV, since the energy deposited by the emitted proton and α-particle is linearly proportional to

the kinetic energy of the impinging neutron. A recent paper has evaluated the capabilities of CLYC-6 and CLYC-7 for the detection and characterization of Special Nuclear Materials (SNM) [9].

In this work CLYC-6 and CLYC-7 crystals were characterised for application as a thermal neutron counter and as a fast neutron spectrometer, respectively, in view of their possible integration in the novel B-RAD radiation survey meter. The B-RAD is novel handheld instrument jointly developed and patented by CERN and the Polytechnic of Milan [10,11] and now commercially available from ELSE Nuclear [12], specifically designed to work in regions of high magnetic fields. It consists of a $LaBr_3$ crystal coupled with a Silicon photomultiplier array for photon dose rate measurements and γ-spectrometry. Additional probes are under development and CLYC has been selected as a potential candidate for neutron detection.

In particular, the n/γ discrimination capability, the energy resolution and the quenching factor for the thermal neutrons produced by the $^{6}Li(n,t)\alpha$ reaction in CLYC-6 were measured with a mono-energetic neutron beam from a Deuterium-Deuterium (D-D) generator. For CLYC-7, the n/γ discrimination and the quenching factor of the $^{35}Cl(n,p)^{35}S$ reaction were measured with the same neutron beam. The fast neutron spectrometric capability of CLYC-7 was also investigated with the continuum neutron spectra from Am-Be and ^{252}Cf sources.

In [4], the response of CLYC-7 to monoenergetic neutrons showed promising results as a spectrometer, since the energy peak coming from the $^{35}Cl(n,p)^{35}S$ reaction was still detected up to 8 MeV. However, above 2.5 MeV a second peak due to the (n,α) reaction is present [4], and the spectrum degenerates in a continuum above 5.5 MeV. Therefore, as already underlined in [13], fast neutron spectrometry with CLYC-7 in presence of a continuum spectrum is quite difficult already above 2.5 MeV. Figure 1 shows the cross sections of the main reactions occurring in CLYC-7 below 14 MeV. The plot shows that the energy threshold for the (n,α) reaction and for the (n,p) reactions to the excited states of ^{35}S is around 2 MeV. Above 4 MeV the cross sections are not negligible, *i.e.*, neutrons with the same energy undergo competing nuclear reactions and the univocal correlation between the initial neutron energy and the energy deposited by the emitted particle is lost.

In this work we exploited the different Linear Energy Transfer (LET) of protons and α-particles to perform proton/α-particle (p/α) discrimination via the PSD method. A preliminary analysis was made with Am-Be and ^{252}Cf sources demonstrating the feasibility of the analysis at least up to 5 MeV. However, due to the small difference of their LET, the proton and α-particle distributions in the 2D PSD plot are not completely separated. This limitation can be overcome with a more sophisticated PSD analysis and/or specifically designed electronics (e.g. shaper or analog PSD) and/or a faster photodetector.

On the other side, CLYC-6 cannot be employed as a spectrometer because the acquired neutron spectrum is usually dominated by a narrow peak due to the $^{6}Li(n,t)\alpha$ reaction from thermal neutrons. However, its large cross section makes it suitable for thermal neutron detection and an appealing alternative to the commonly used ^{3}He proportional counter, especially because of the diminishing stockpile of ^{3}He gas [14].

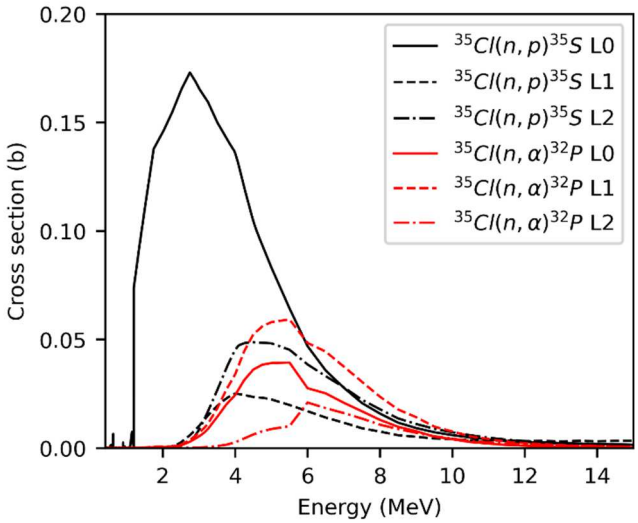

Figure 1. The (n,p) and (n,α) reaction cross sections on ^{35}Cl, where L0 stands for the ground state and L1 and L2 for the first and second excited states. Data are taken from the ENDF/B VIII.0 library [15].

2. Materials and methods

Both CLYC-6 and CLYC-7 crystals were grown by Radiation Monitoring Devices Inc. (RMD) [16]. The former (serial number 730-3D1, April 2020) is a parallelepiped with dimensions of 18 ×18 ×5 mm^3, enriched in ^6Li to > 95%. The latter (serial number 039-2, September 2017) is a 1–inch right cylinder enriched in ^7Li to > 99%. Both crystals were wrapped with a reflective inner coating and encapsulated in an aluminium casing. The energy resolution at 662 keV declared by the manufacturer is < 5% FWHM for both crystals.

Each crystal was coupled with a R6231-100 Superbialkali Hamamatsu Photomultiplier Tube (PMT) [17] operating at 1,100 V through optical grease, and placed inside a light–tight box. The output signal was directly sent to a 1 GHz, up to 2.5 Gs/s, 12 bit HDO6104 Teledyne Lecroy Oscilloscope, by a 50 Ω termination. The sampling frequency in this work was set to 250 Ms/s. Each signal was saved and offline analysed with a Python code [18]. For the measurement of the neutron detection efficiency of CLYC-6 (section 3.4) a CAEN DT5720 digitizer (12 bit, 250 Ms/s) was used in place of the oscilloscope, because it allows faster signal processing and is provided with the DPP-PSD software for on-line PSD analysis (which was used instead of the Python analysis).

Before each measurement, the experimental set-up was energy calibrated with γ-ray sources of different energies (^{137}Cs and either ^{60}Co or ^{22}Na). The charge spectrum of each γ-ray source was acquired by calculating the charge of each signal as the pulse integral over the first 8 µs. The charge to energy equation was calculated by linear fitting of the data points corresponding to each photoelectric peak.

In order to discriminate neutrons from γ-ray events, the PSD analysis was performed by means of the Charge Integration Method [19,20]. Two different time windows were selected, the first from 0 s to t = t_{prompt} and the second from t_{prompt} to t = t_{delay}, where t_{prompt} and t_{delay} are two selected times of the pulse tail. The integrals of the signals along the corresponding intervals were calculated and labelled as Q_{prompt} and Q_{delay} respectively. The PSD was calculated as the ratio Q_{delay} / (Q_{prompt} + Q_{delay}). Because of the different time profiles of the pulses generated by neutrons and γ-rays, the PSD histogram plot defines two Gaussian distributions ascribed to the two kinds of radiation. Each

distribution was fitted using a Gaussian equation and a Figure-of-Merit (FOM) was calculated to evaluate the goodness of the PSD. The FOM was defined as follows:

$$\mathrm{FOM} = \frac{x_n - x_\gamma}{FWHM_n + FWHM_\gamma} \quad (1)$$

where x_γ and x_n are the peak centroids of the photon and neutron Gaussian distributions and $FWHM_\gamma$ and $FWHM_n$ the corresponding full widths at half maximum. The n/γ PSD was performed by always setting the time windows t_{prompt} and t_{delay} to 70 ns and 2 µs respectively, unless otherwise specified in the corresponding section. The values of t_{prompt} and t_{delay} were selected as the time windows that optimise the FOM.

A Thermo Scientific MP 320 Deuterium-Deuterium (D-D) generator [21] emitting 2.5 MeV neutrons was used for the measurements of the n/γ discrimination, energy resolution and quenching factor. The neutron energy resolution of CLYC-7 was not calculated because of a sudden degradation of the crystal, which only concerns the measurements with the D-D generator (section 4.1 and 4.2). All other measurements (with the Am-Be and ^{252}Cf sources) were performed before the worsening of the crystal's performance. As an example, the energy calibrated spectra of ^{137}Cs and ^{60}Co and the corresponding energy resolutions, acquired simultaneously with the measurements described in section 4.4 are shown in figure 2 (left). For completeness, figure 2 (right) shows the ^{137}Cs and ^{22}Na spectra and the corresponding energy resolutions obtained with CLYC-6 simultaneously with the measurements described in section 3.1. The energy resolution is worse than the reference one (9% for CLYC-7 and 7% for CLYC-6 at 662 keV versus < 5% declared by the company). The energy calibration applied in figure 2 was calculated by integrating the signals over 2 µs, selected as the integration time between 500 ns and 8 µs that optimises the energy resolution. The energy calibration used for the calculation of the neutron spectra was calculated instead by setting the same integration time for both the γ-ray and the neutron sources. The reason of the worse energy resolution might be the digital electronics, an analog shaping electronics (*e.g.* preamplifier, amplifier and multi-channel analyser as suggested by the company) might improve the energy resolution by 2% [5]. In addition, we cannot exclude a degradation of the performance of the PMT, and for CLYC-7 of the crystal itself and/or of his housing (CLYC is highly hygroscopic) since they were purchased three years before these measurements and used for several past tests. The neutron detection efficiency of CLYC-6 was measured with the thermal neutron field available at the Calibration Laboratory (Cal Lab) of CERN Radiation Protection group [22]. The study of CLYC-7 as a fast neutron spectrometer was performed by irradiating the crystal with neutrons from both an Am-Be source and a ^{252}Cf source.

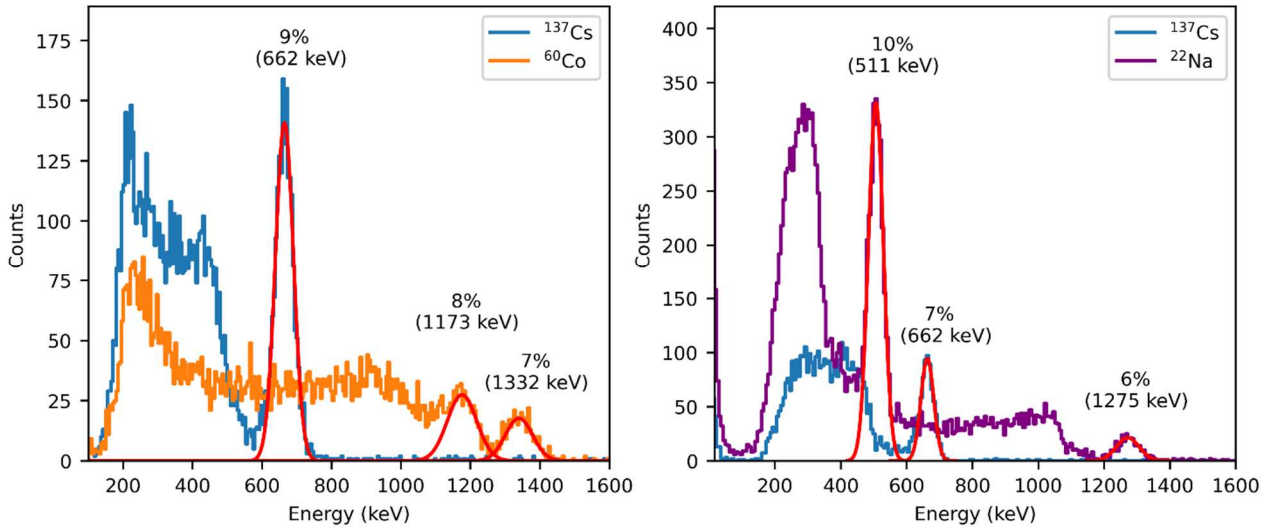

Figure 2. Left: ^{137}Cs and ^{60}Co energy calibrated spectra acquired with CLYC-7 when irradiated with Am-Be source neutrons. Right: ^{137}Cs and ^{22}Na energy calibrated spectra acquired with CLYC-6 when irradiated with 2.5 MeV source neutron. The energy resolution of each photopeak is indicated.

3. Measurements with CLYC-6

3.1. n/γ discrimination capability

Figure 3 shows the 1D and 2D histogram plots of the PSD and PSD versus energy acquired with CLYC-6 and the D-D generator. The calculated FOM is 2.20 (for 100 keVee energy threshold), which confirms the excellent n/γ discrimination capability of the crystal. The 2D PSD plot clearly shows the separation between the neutron events (on top of the plot) and the γ-ray events (on the bottom) with no overlap between the two distributions. The neutron distribution is dominated by a blob at around 3 MeVee corresponding to the $^{6}Li(n,t)\alpha$ reaction from thermal neutrons [7,13,23]. A single narrow energy peak is seen in the neutron spectrum (see figure 4) as discussed in the next section.

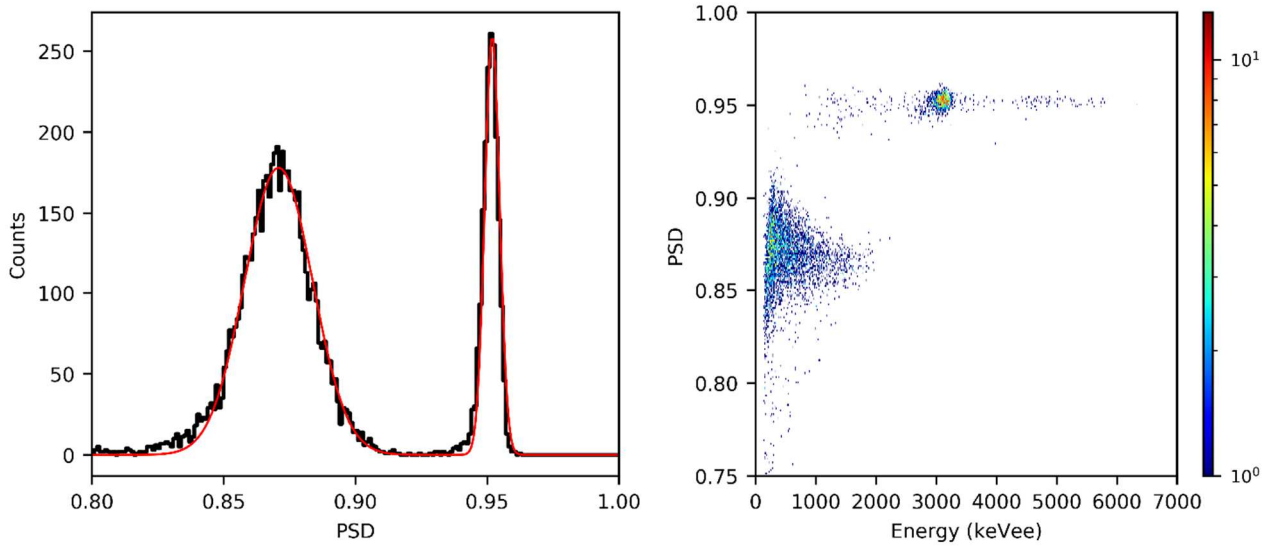

Figure 3. Left: the 1D PSD histogram plot acquired with CLYC-6 irradiated with 2.5 MeV neutrons from a D-D generator. The red line is the Gaussian fit to the γ-ray (left peak) and neutron (right peak) distributions. Right: the 2D PSD plot for the same measurement.

3.2. Neutron spectrum and energy resolution

From the PSD analysis the neutron events were selected and plotted in terms of counts versus energy, after the energy calibration. Figure 4 shows the resulting neutron spectrum acquired with the D-D generator. The main peak is attributed to the thermal neutron absorption on ^{6}Li. Thermal neutrons are probably produced by the scattering of the 2.5 MeV source neutrons with the surroundings. The 2.5 MeV source neutrons can also directly interact with CLYC-6 via the ^{6}Li(n,t)α reaction. These events should appear on the right-end side of the thermal peak [7], however due to the difference between the thermal and fast neutron cross sections (940 b at 25 meV versus 0.17 b at 2.5 MeV), the thermal peak is dominant. Neutrons of 2.5 MeV are also detected via the ^{35}Cl(n,p)^{35}S reaction (the cross section for 2.5 MeV neutrons is 0.19 b) as a single energy peak at 2.5 MeV + the Q-value of the reaction, multiplied by the proton quenching factor equal to 0.9 (see section 3.3 for the definition and section 4.2 for the calculation and references), i.e. at 2.8 MeV. The corresponding peak should appear at the left of the thermal neutron peak and can be the origin of the small bump visible just below the thermal peak [7,8].The detected peak was fitted using a Gaussian fitting equation and the energy resolution calculated as the ratio between the corresponding FWHM and the mean value of the peak. The thermal neutron energy resolution is 6%.

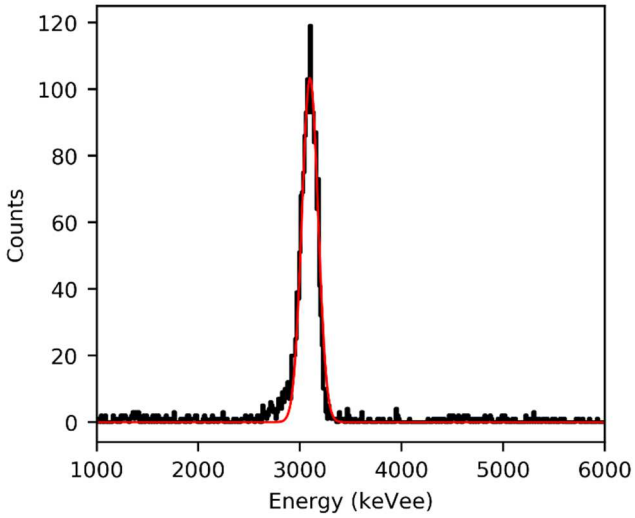

Figure 4. The neutron spectrum acquired with CLYC-6 irradiated with 2.5 MeV neutrons from a D-D generator. The red line is the Gaussian fit to the peak corresponding to the ^{6}Li(n,t)α reaction.

3.3. Quenching factor of the ^{6}Li(n,t)α reaction

The quenching factor q is defined as:

$$q = \frac{E_{eq.}}{E_N + Q} \quad (2)$$

where $E_{eq.}$ is the energy in equivalent electron-volt (eVee) of the reaction, E_N the energy in electron-volt of the impinging neutron and Q the Q-value of the reaction in electron-volt. In this case, E_N is negligible (*i.e.*, thermal energy) and the Q-value is 4.78 MeV. $E_{eq.}$ was calculated as the mean value of the Gaussian fit of the peak in the neutron spectrum (figure 4), *i.e.,* 3.1 MeV. The resulting q is 0.65 in agreement with [24] which reports a value of 0.7 for the ^{6}Li(n,t)α reaction.

3.4. Neutron detection efficiency

A tailored cut polyethylene cylinder was placed around the Am-Be source of Cal Lab. The cylinder moderates the fast neutrons emitted by the source and produces a thermal neutron field that irradiated the CLYC-6 crystal [22]. The crystal was placed at 86 cm from the source at the same height above the floor, aligned with two orthogonal lasers. The neutron count rate was obtained after the PSD analysis. For comparison, the neutron count rate at the same irradiation position was measured with a Centronic SP9/152/Kr ^{3}He proportional counter (17 cm^3 sensitive volume), filled with a gas mixture of ^{3}He at 2.33 kPa (2.3 atm) and Kr at 1.22 kPa (1.2 atm). The counter was supplied with +820 V and the output signal processed by an ORTEC 142IH preamplifier, an ORTEC 570 amplifier (assembled in a portable NIM crate) and an Amptek Pocket Multi-Channel Analyser 8000D. The neutron count rate was measured integrating the recoil spectrum acquired by the multi-channel analyser setting a proper energy threshold to cut the electronic noise and γ-ray events.

Taking into account the sensitive volume of each detector, the measurements confirmed that the neutron detection efficiency per unit volume (cm^3) of CLYC-6 is higher than that of the ^{3}He counter [14], 50 counts per second (cps) per cm^3 with CLYC-6 (1.62 cm^3) versus 20 cps per cm^3 with the ^{3}He counter (17.15 cm^3).

4. Measurements with CLYC-7

4.1. n/γ discrimination capability

Figure 5 shows the 1D and 2D histogram plots of the PSD and PSD versus energy acquired with CLYC-7 irradiated with the D-D generator. The Gaussian fits of the neutron and γ-ray distributions are also plotted in figure 5. The corresponding FOM is 2.04, demonstrating excellent n/γ discrimination. The FOM for CLYC-7 is slightly lower than for CLYC-6 in agreement with [9].

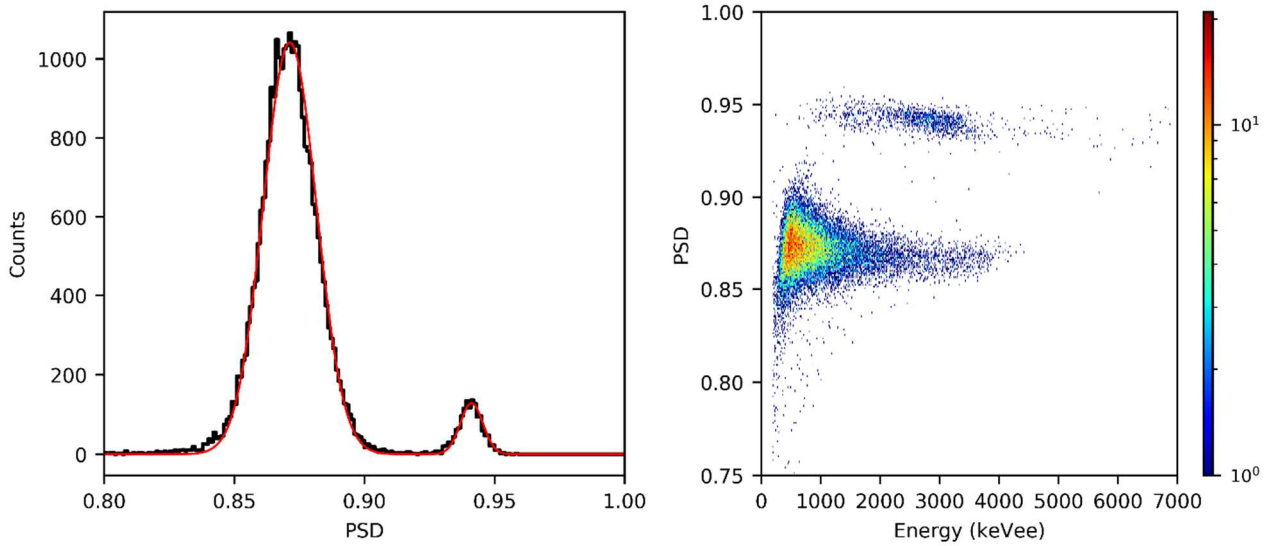

Figure 5. Left: the 1D PSD histogram plot acquired with CLYC-7 irradiated with 2.5 MeV neutrons from a D-D generator. The red line is the Gaussian fit to the γ-ray (left peak) and neutron (right peak) distributions. Right: the 2D PSD plot for the same measurement.

4.2. Quenching factor of the ^{35}Cl(n,p)^{35}S reaction

Figure 6 shows the neutron spectrum acquired with CLYC-7 irradiated with 2.5 MeV neutrons from the D-D generator. The main peak at 2.83 MeVee is due to the (n,p) reaction on ^{35}Cl, the counts detected at the left of the main peak (at around 1.1 MeVee and 1.7 MeVee) come from the (n,α) reaction [13] (to the ground and to the first excited state of ^{32}P) and the (n,p) reaction to the excited states of ^{35}S. Some counts in this energy range can also derive from scattered neutron background. The quenching factor for the ^{35}Cl(n,p) reaction was calculated using equation (2), where $E_{eq.}$ is the centroid of the Gaussian fit to the 2.83 MeVee peak shown in figure 6, E_N = 2.5 MeV and Q = 0.615 MeV. A value of 0.91 was found, in perfect agreement with literature data (from 0.85 to 0.92 in [13], 0.9 in [24]).

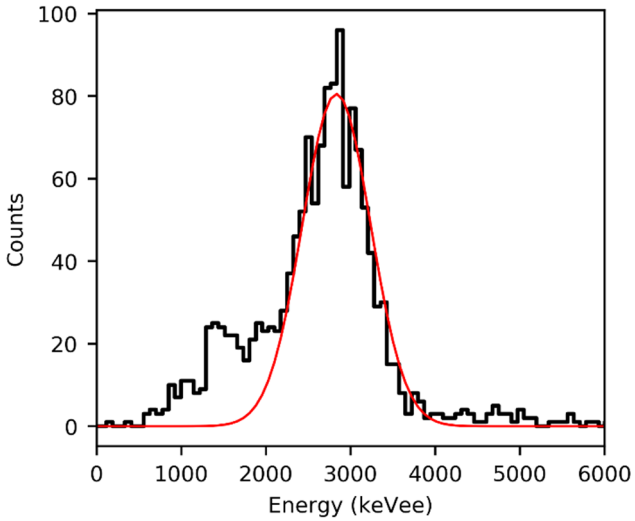

Figure 6. Neutron energy spectrum acquired with CLYC-7 irradiated with 2.5 MeV neutrons from a D-D generator. The red line is the Gaussian fit to the peak at 2.83 MeVee corresponding to the ^{35}Cl(n,p)^{35}S reaction.

4.3. The Am-Be neutron spectrum

CLYC-7 was irradiated with Am-Be source neutrons. The n/γ PSD analysis was first performed as in the previous study to discard the γ-ray events. Figure 7 shows the 2D histogram plot of the PSD versus energy where the red line delimits the neutron and γ-ray regions in the PSD space. The distance between x_γ and the red line is larger than $3\sigma_\gamma$, where x_γ and σ_γ are the centroid and the standard deviation of the Gaussian equation fitting the γ-ray distribution. Few signals were detected in between the neutron and γ-ray distributions. Because of the uncertainty associated to these signals, they were discarded from the analysis. It is worth mentioning that these signals are 7% of the total neutron signals and are spread over about 5 MeV. Their effect on the resulting neutron

spectrum is negligible (the neutron spectrum with these signals differs by less than 1% compared with the spectrum without).

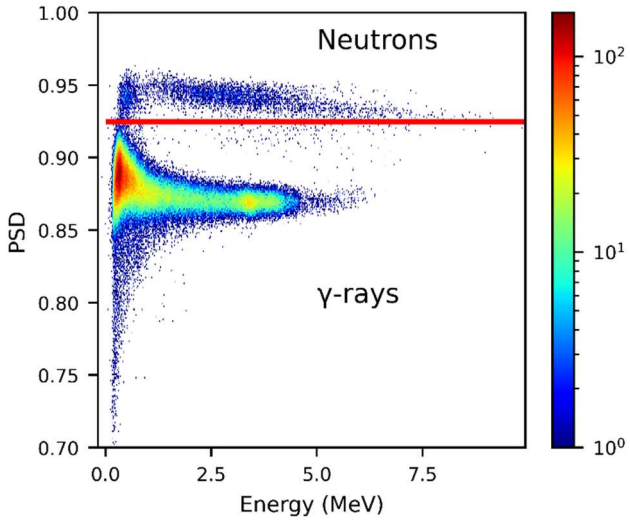

Figure 7. 2D histogram plot of the PSD versus energy for CLYC-7 irradiated with Am-Be source neutrons.

The γ-ray events were discarded, and the PSD analysis was repeated on the selected neutron signals by varying t_{prompt} from 10 ns to 1.5 µs while t_{delay} was kept constant at 2 µs. Figure 8 shows the 2D histogram plots of the PSD versus energy for the different values of t_{prompt}, as indicated in each plot. The width of the binning and the scale of the x-axis are the same for all plots, while the y scale changes to better visualise the region of interest of each plot. For larger t_{prompt} values (bottom plots) the neutron signals follow a unique distribution. By decreasing the value of $t_{prompt,}$ the neutron distribution starts to broaden and below 100 ns a second distribution arises that deviates from the main distribution. This trend indicates that the signals differ in the first part of their time profile. Variations on the first part of the signals become indeed negligible for larger values of t_{prompt}, when t_{prompt} is almost equal to t_{delay}.

This second distribution appears at higher PSD values, which means that it is composed of slightly slower signals (as defined in section 2). For this reason, we associated this distribution to α-particle events: α-particles are higher LET particles (*i.e.,* slower signal) as compared to protons. The α-particle distribution should appear starting from about 2 MeV. At this energy, its cross section is negligible compared with the (n,p) cross section (less than 1%). However, due to the small difference of their signal profiles, the two distributions overlap between 2 MeV and up to around 4 MeV. Only above this energy two distributions can be identified.

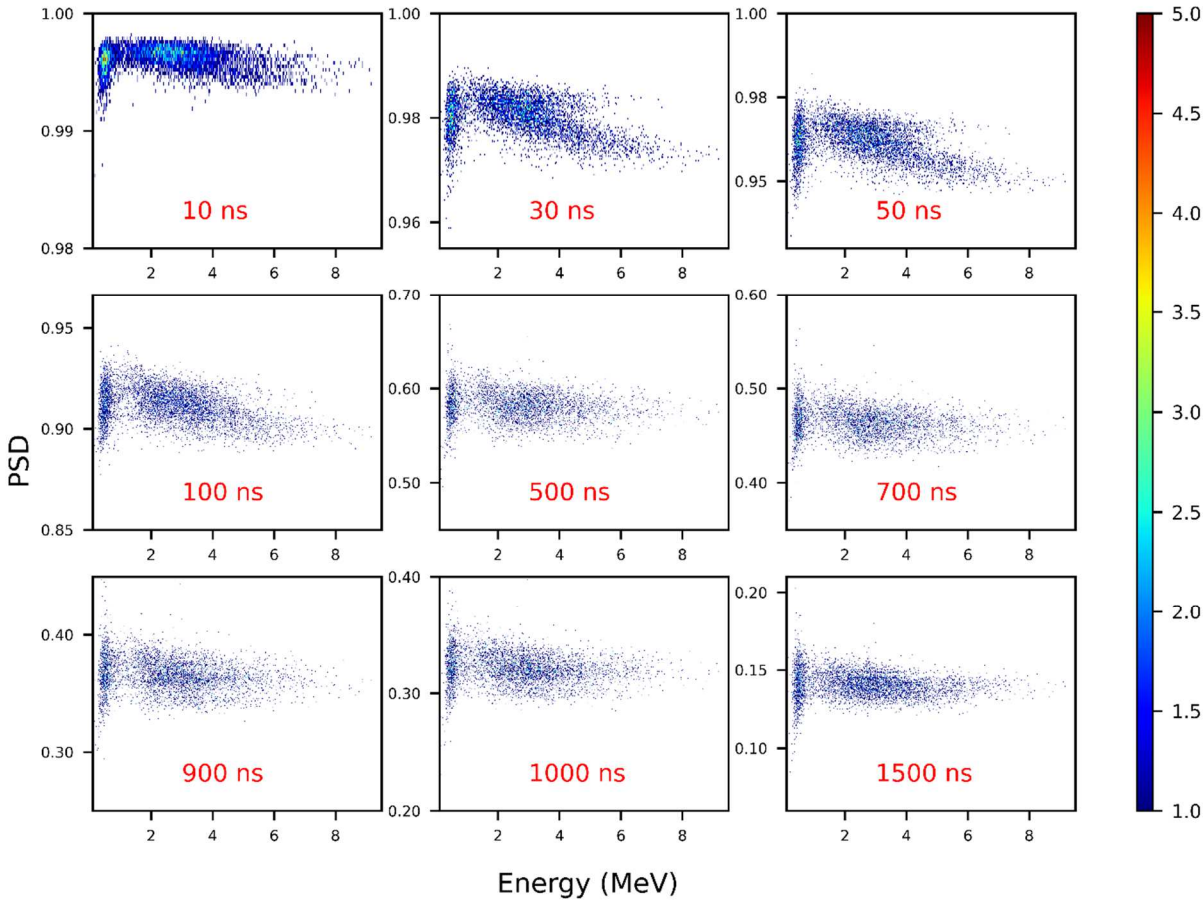

Figure 8. 2D histogram plots of the PSD versus energy for CLYC-7 of the neutron signals from an Am-Be source at different t_{prompt}. The value of t_{prompt} is indicated in each plot, whilst t_{delay} is constant (2 μs).

For each value of t_{prompt}, the PSD values corresponding to the neutron signals were plotted into a histogram, selecting only the signal with E > 4 MeV. For t_{prompt} equal to 30 ns and 50 ns only, two Gaussian-like distributions appear which were fitted using a Gaussian equation, and the FOM calculated as follows:

$$\text{FOM} = \frac{x_\alpha - x_p}{FWHM_\alpha + FWHM_p} \quad (3)$$

where x_α and x_p are the peak centroids of the α-particle and proton Gaussian distributions and $FWHM_\alpha$ and $FWHM_p$ the corresponding full widths at half maximum. The calculated FOM was 0.68 and 0.75 for 30 ns and for 50 ns respectively. The latter was thus selected for the p/α discrimination. Figure 9 compares the PSD histogram plot obtained for t_{prompt} = 500 ns and t_{prompt} = 50 ns. The separation between the proton and the α-particle distributions is not very good (a FOM < 1.25 implies that $x_\alpha - x_p < 3\,(\sigma_\alpha + \sigma_p)$), however two distributions have been detected, while it was not possible for other t_{prompt} values (such as for t_{prompt} =500 ns, as shown in figure 9).

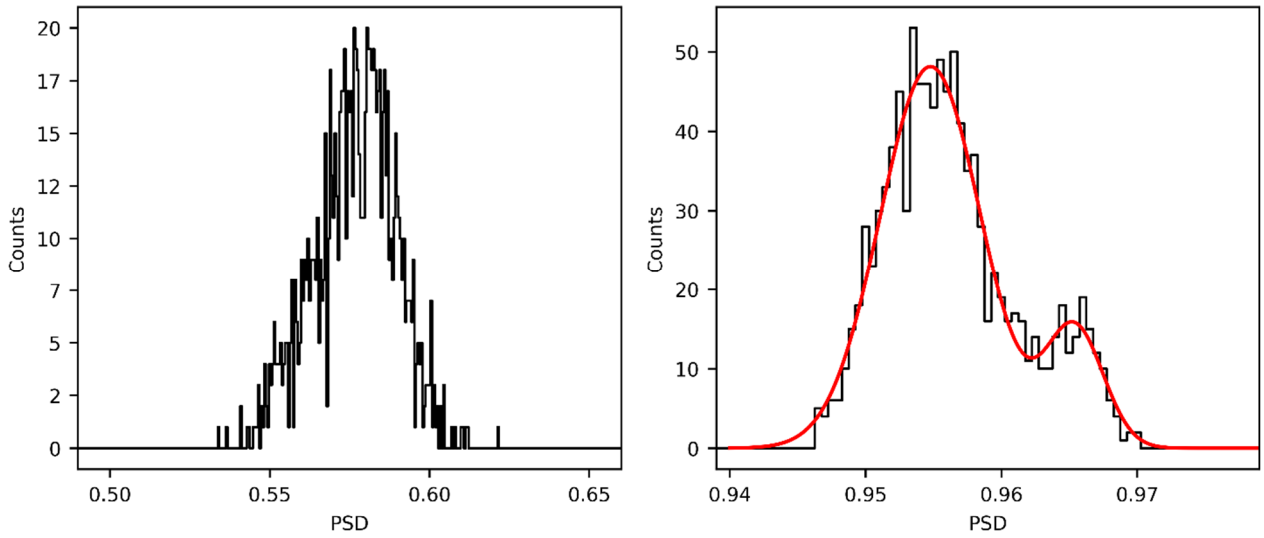

Figure 9. The 1D histogram plot of the PSD for CLYC-7 for the neutron signals at t_{prompt} = 500 ns (on the left) and t_{prompt} = 50 ns (on the right). The right plot also shows the Gaussian fit to the selected proton and α particle distributions.

A PSD cut-off value equal to 0.9622 was defined, below which the pulses were classified as produced by protons and above by α-particles, excluding from the α-particles all signals detected as a blob below 1.5 MeV which spread over a wider PSD range (0.95-0.98). The latter are instead classified as protons since the (n,α) cross section is negligible below 1.5 MeV (0.10977 b the (n,p) cross section versus 0.0005 b the (n,α) cross section at 1.5 MeV [15]). According to this criterion, the pulses from protons and α-particles were collected separately and plotted into a histogram. The spectra so calculated correspond to the spectra of the energy deposited by protons and α-particles respectively, as a function of $E_{eq.}$. We will refer to them as $S_p(E_{eq.})$ and $S_\alpha(E_{eq.})$.

Inverting equation (2), the corresponding neutron spectra can be calculated as follows:

$$E_N = \left(E_{eq.}/q\right) - Q \tag{3}$$

The neutron energy spectra, labelled as $S_p(E_N)$ and $S_\alpha(E_N)$, were calculated applying equation (3) to $S_p(E_{eq.})$ and $S_\alpha(E_{eq.})$, assuming q equal to 0.9 (see section 4.2) for protons and to 0.5 for α particles [24]. The Q_{value} is 615 keV for the (n,p) reaction and 938 keV for the (n,α) reaction.

Figure 10 shows $S_p(E_{eq.})$ and $S_p(E_N)$, figure 11 $S_\alpha(E_{eq.})$ and $S_\alpha(E_N)$.

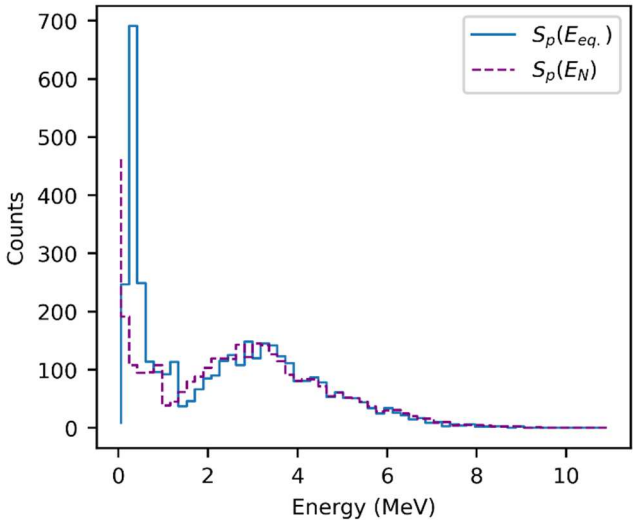

Figure 10. The spectrum of the energy deposited by protons in CLYC-7 (continuous blue line) and the related spectrum of the incoming neutrons (dotted purple line), calculated taking into account the quenching factor (0.9) and the Q-value of the reaction (615 keV).

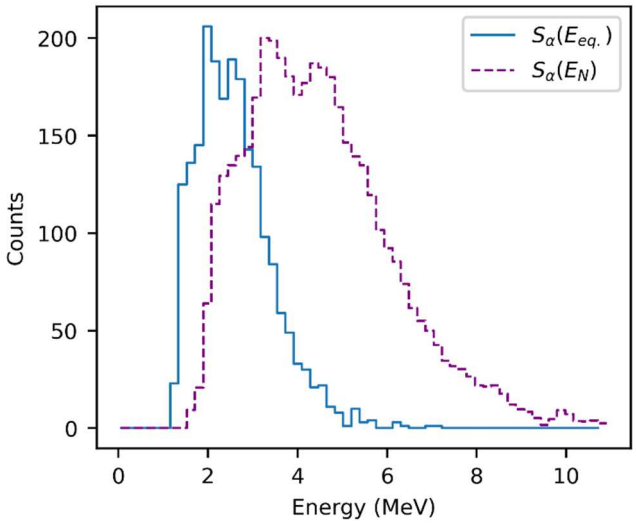

Figure 11. The spectrum of the energy deposited by α particles in CLYC-7 (continuous blue line) and the related spectrum of the incoming neutrons (dotted purple line), calculated taking into account the quenching factor (0.5) and the Q-value of the reaction (938 keV).

The total spectrum of the incoming neutrons was calculated as the sum of $S_p(E_N)$ and $S_\alpha(E_N)$ and is compared with the ISO spectrum [25] and with the spectrum calculated without the p/α discrimination in figure 12. The three spectra have been normalised to their maximum (discarding the energy bins below 500 keV). Figure 12 also shows the percent difference ($d_{\%}$) between the Am-Be ISO spectrum and the spectrum with and without the p/α discrimination. $d_{\%}$ is defined as:

$$d_{\%} = \frac{|y_{ISO,i} - y_i|}{y_{ISO,i}} \times 100 \quad (4)$$

where $y_{ISO,i}$ is the intensity of the normalised Am-Be ISO spectrum in the i-th bin and y_i the normalised counts of the experimental spectrum for the same bin. The average $d_{\%}$ for E > 500 keV

(*i.e.* for fast neutron energies) is 46% with the p/α discrimination and 68% without the p/α discrimination.

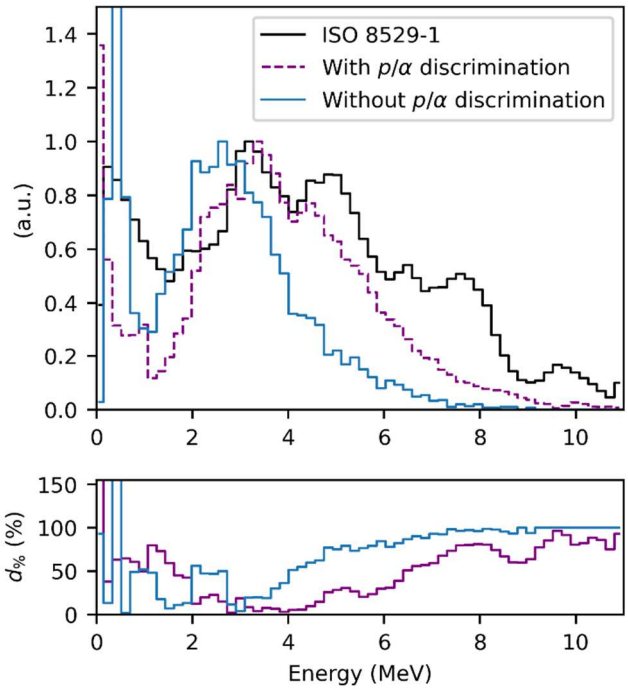

Figure 12. Top: comparison between the Am-Be ISO spectrum (continuous black line) and the neutron spectrum measured with CLYC-7, without discrimination of neutron signals (continuous blue line) and with the p/α discrimination (dotted purple line). Bottom: percent variation between the Am-Be ISO spectrum and the spectrum obtained with (continuous purple line) and without (continuous blue line) p/α discrimination.

4.4. The ^{252}Cf neutron spectrum

The procedure described in section 4.3 was applied to the data acquired irradiating CLYC-7 with ^{252}Cf source neutrons. For this case only, t_{delay} were set to 1.5 µs while t_{prompt} was kept at 70 ns for the n/γ discrimination and at 50 ns for the p/α discrimination. Figure 13 compares the ISO spectrum [25] and the experimental spectrum before and after the analysis proposed in this work. The resulting $d_{\%}$ parameters for E > 500 keV were 61% and 77% with and without the p/α discrimination respectively.

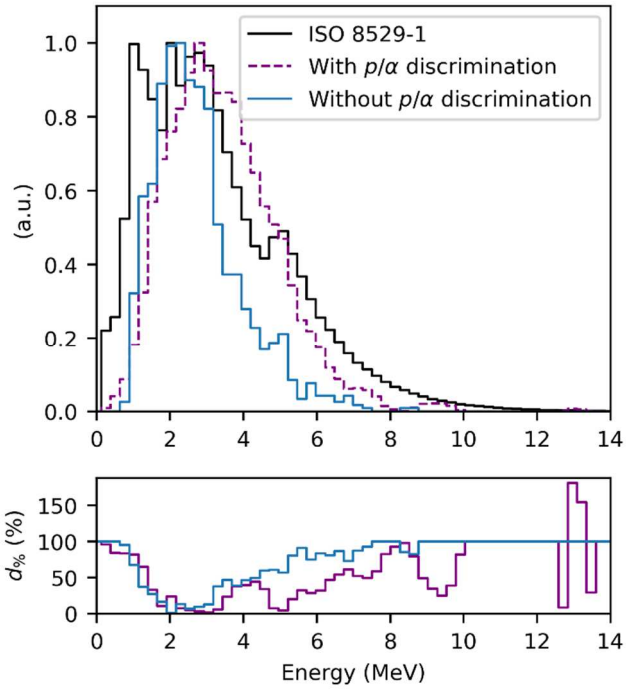

Figure 13. Top: comparison between the ^{252}Cf ISO spectrum (continuous black line) and the neutron spectrum measured with CLYC-7, without discrimination of neutron signals (continuous blue line) and with the p/α discrimination (dotted purple line). Bottom: the percentage variation between the ^{252}Cf ISO spectrum and the spectrum obtained with (continuous purple line) and without (continuous blue line) the p/α discrimination.

4.5. Pulse shape analysis of the neutron signals

To quantify the difference in terms of time profile between the proton and α-particle signals defined by the p/α discrimination proposed in this work, a pulse shape analysis was performed. The signals acquired with the CLYC-7 irradiated with the Am-Be source were considered and the so-called standard pulse of protons and α-particles was calculated as follows. All signals were aligned and the PSD was calculated as described in section 2 (t_{prompt} = 70 ns and t_{delay} = 2 µs). The γ-ray signals, *i.e.* the signals below the red line in figure 7, were discarded and the p/α discrimination was applied to the remaining signals as described in section 4.3 (t_{prompt} = 50 ns and t_{delay} = 2 µs). Only the events with E > 4 MeV were selected, where the recognised proton and α-particle distributions do not overlap (see figure 8, case t_{prompt} = 50 ns). The pulses recognised as protons were averaged and normalised to obtain the proton standard pulse. The same calculation was performed to obtain the α-particle standard pulse. Figure 14 shows the results.

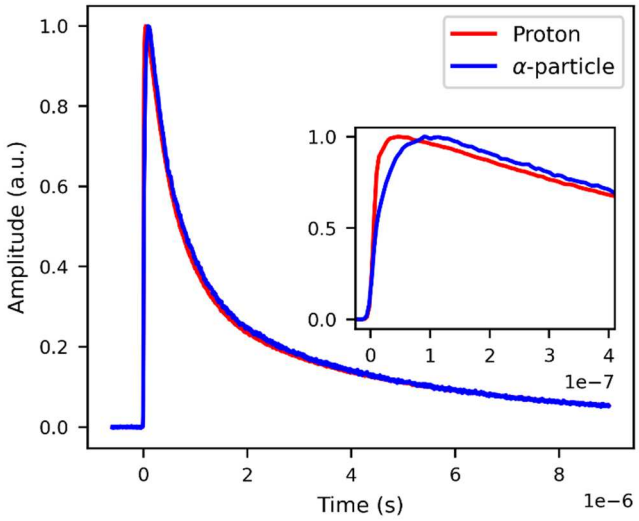

Figure 14. The proton and α-particle standard pulses obtained with the proposed p/α discrimination, in CLYC-7 irradiated with Am-Be source neutrons

4.6. Discussion on the p/α discrimination

The p/α discrimination via the PSD method is in principle possible. In fact, with the properly selected time windows, different kinds of particles are collected in different distributions in the PSD plot. Giaz *et al* [3] also detected two different distributions irradiating CLYC-7 with 14.1 MeV neutrons. The two distributions were also attributed to different LET particles, *i.e.*, protons and α particles. However, Giaz *et al.* did not exploit this difference to improve the CLYC spectroscopic capability. A similar analysis was instead proposed by Dolympia *et al* [4] with a 7.23 MeV monoenergetic neutron beam. However, a continuous neutron spectrum, as used in this work, represents a more realistic scenario.

The pulse shape analysis demonstrates the correctness of the method since the signals ascribed to protons are faster than the signals ascribed to α-particles, *i.e.* the PSD is able to distinguish even small differences in the time profile if the proper time windows are selected. This was also demonstrated for higher neutron energies (up to 60.5 MeV) in [5]. For this case, the proton and α-particle's standard pulses differ the most in the first 100 ns of the signal, during their rise time. The rise time of the proton and α-particle standard pulses is 16 ns and 48 ns respectively. The tails of the two signals are slightly different up to around 4 µs. However, the corresponding fall times are more comparable, 5.38 µs for protons and 5.54 µs for α-particles.

After the p/α discrimination the measured Am-Be and ^{252}Cf spectra better match the corresponding ISO spectra. The percent difference between the experimental and the ISO spectra, averaged over the spectrum energies, improves for both cases by more than 15% when the p/α discrimination is applied. Above 2 MeV the spectrum with p/α discrimination is always closer to the corresponding ISO spectrum than the spectrum without discrimination (except at 13 MeV for two bins for the ^{252}Cf source). However, above 5 MeV the difference between ISO and experimental spectra increases in both cases, probably because of the drop of the (n,p) cross section at 5 MeV and the increasing importance of different reaction channels (see figure 1).

The non-match between the reference spectrum and the experimental one, in particular below 3-4 MeV, is due to the uncertainty associated with the p/α discrimination since, in this region, many proton and α-particle pulses overlap. For Am-Be, a high peak at low energy is also visible, which can be due to either the scattered neutron component [3] or the resonance peaks of the (n,p) cross

section below 1 MeV [23] (figure 15). Because of the lack of thermal neutrons in the ^{252}Cf spectrum, the same peak is not revealed.

The ^{252}Cf neutron spectrum has a more pronounced low energy component as compared to the Am-Be spectrum and, as a consequence, the shape of the experimental spectrum without the p/α discrimination already matches quite well the peak of the ISO spectrum between 2 MeV and 3 MeV [6]. However, the tail of the spectrum is not well reproduced, whilst the p/α discrimination partially restores the correct shape above 3 MeV.

Despite the p/α discrimination performed in this study improves the performance of CLYC-7 as a spectrometer, the method is still not rigorous since the overlapping region between the proton and α-particle is dominant and the selection of the discrimination parameter is affected by high uncertainty. A second limitation exists which cannot be overcome: the contribution to the neutron spectrum of the (n,p) and (n,α) reactions leaving the ^{35}S and ^{32}P in their excited states. These reactions contribute to the neutron spectrum also below 8 MeV, depositing per event less energy compared with the corresponding reaction leaving the ^{35}S and ^{32}P to the ground states. However, protons emitted by the (n,p) (ground state) reactions cannot be distinguished by protons emitted after the (n,p) (excited state) reactions. The same is valid for α-particles. In general, the analysis must be improved for example with the use of a faster photodetector, a specific electronic readout or a more sensitive PSD analysis, and further investigations are needed before its application. Nevertheless, the application of CLYC-7 as a portable fast-neutron spectrometer for the B-RAD detector, is still attractive. A small, lightweight, single detector, instead of the commonly used Bonner Sphere Spectrometer, represents a great advantage especially in some applications in radiation protection where some uncertainty is acceptable.

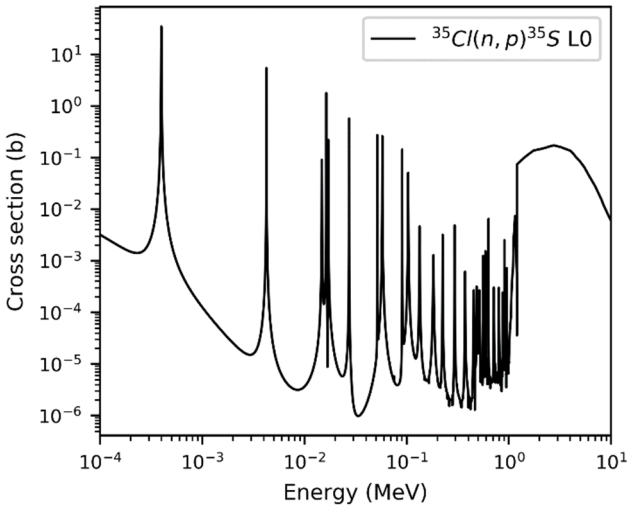

Figure 15. Zoom of the total cross section of the (n,p) and (n,α) reactions on ^{35}Cl, in the region of interest. Below 1 MeV several resonance peaks are visible [15].

5. Conclusions

CLYC-6 (enriched in ^{6}Li to > 95%) and a CLYC-7 (enriched in ^{7}Li to > 99%) crystals were studied as thermal neutron detector and as fast neutron spectrometer, respectively. Both crystals were irradiated with a 2.5 MeV monoenergetic neutron beam and their n/γ discrimination capability evaluated by the PSD method, both showing excellent performance (FOM > 2). The energy

resolution of CLYC-6 to 2.5 MeV neutrons is 6% and the measured quenching factor for the $^{6}Li(n,t)\alpha$ reaction is 0.65. The quenching factor of the $^{35}Cl(n,p)^{35}S$ reaction in CLYC-7 is 0.91.

As neutron counter, the thermal neutron detection efficiency of CLYC-6 was measured relative to that of a ^{3}He proportional counter. For the thermal neutron field available at Cal Lab and for the same irradiation position, CLYC-6 shows a 60% higher efficiency per unit volume.

The neutron spectrometry capability of CLYC-7 was investigated irradiating the crystal with the continuum neutron spectra from Am-Be and ^{252}Cf sources. A p/α discrimination was carried out by the PSD method, to distinguish between the protons and α-particles produced by the two main reactions occurring in the crystal below 10 MeV. After p/α discrimination the experimental neutron spectra better match the corresponding ISO spectra above 2 MeV. The best match was found between 2 MeV and 4 MeV, where the difference with the ISO spectrum is below 30%. Below 2 MeV, the overlapping of proton and α-particle pulses is not negligible, whilst above 5 MeV different reaction channels become comparable with the abovementioned ones.

The results here reported show that CLYC-7 is a suitable candidate for a probe for fast neutron spectrometry for B-RAD below ~ 5 MeV and, simultaneously, as a stationary environmental detector to monitor both the γ-ray (with the current probe [12]) and the neutron dose rates. However, the proposed p/α discrimination method cannot yet be applied in an actual detector as many events are still erroneously classified. CLYC-6 can instead be used for neutron count rate and measurement of neutron ambient dose equivalent if embedded in a moderator (typically polyethylene) to increase the thermal neutron component of the neutron field.

Acknowledge

We wish to thank RMD for supplying the CLYC-6 crystal. This project has been partially funded by the CERN Knowledge Transfer fund, through a grant awarded in 2014.

References

[1] J. Glodo, W.M. Higgins, E. V.D. Van Loef, K.S. Shah, Scintillation properties of 1 inch Cs_2LiYCl_6:Ce crystals, IEEE Transactions on Nuclear Science. 55 (2008) 1206–1209. https://doi.org/10.1109/TNS.2007.913467.

[2] N. D'Olympia, P. Chowdhury, C.J. Lister, J. Glodo, R. Hawrami, K. Shah, U. Shirwadkar, Pulse-shape analysis of CLYC for thermal neutrons, fast neutrons, and gamma-rays, Nuclear Instruments and Methods in Physics Research, Section A: Accelerators, Spectrometers, Detectors and Associated Equipment. 714 (2013) 121–127. https://doi.org/10.1016/j.nima.2013.02.043.

[3] A. Giaz, L. Pellegri, F. Camera, N. Blasi, S. Brambilla, S. Ceruti, B. Million, S. Riboldi, C. Cazzaniga, G. Gorini, M. Nocente, A. Pietropaolo, M. Pillon, M. Rebai, M. Tardocchi, The CLYC-6 and CLYC-7 response to γ-rays, fast and thermal neutrons, Nuclear Instruments and Methods in Physics Research, Section A: Accelerators, Spectrometers, Detectors and Associated Equipment. 810 (2016) 132–139. https://doi.org/10.1016/j.nima.2015.11.119.

[4] N. Dolympia, P. Chowdhury, E.G. Jackson, C.J. Lister, Fast neutron response of ^{6}Li-depleted CLYC detectors up to 20 MeV, Nuclear Instruments and Methods in Physics Research, Section A: Accelerators, Spectrometers, Detectors and Associated Equipment. 763 (2014) 433–441. https://doi.org/10.1016/j.nima.2014.06.074.

[5] R.S. Woolf, A.L. Hutcheson, B.F. Phlips, E.A. Wulf, Response of the Li-7-enriched Cs2LiYCl6:Ce (CLYC-7) scintillator to 6-60 MeV neutrons, Nuclear Instruments and Methods in Physics Research, Section A: Accelerators, Spectrometers, Detectors and Associated Equipment. 803 (2015) 47–54. https://doi.org/10.1016/j.nima.2015.08.080.

[6] N. Dinar, D. Celeste, M. Silari, V. Varoli, A. Fazzi, Pulse shape discrimination of CLYC scintillator coupled with a large SiPM array, Nuclear Instruments and Methods in Physics Research, Section A: Accelerators, Spectrometers, Detectors and Associated Equipment. 935 (2019) 35–39. https://doi.org/10.1016/j.nima.2019.04.099.

[7] M.B. Smith, T. Achtzehn, H.R. Andrews, E.T.H. Clifford, H. Ing, V.D. Kovaltchouk, Fast neutron spectroscopy using Cs_2LiYCl_6:Ce (CLYC) scintillator, IEEE Transactions on Nuclear Science. 60 (2013) 855–859. https://doi.org/10.1109/TNS.2012.2219068.

[8] N. Dolympia, P. Chowdhury, C.J. Guess, T. Harrington, E.G. Jackson, S. Lakshmi, C.J. Lister, J. Glodo, R. Hawrami, K. Shah, U. Shirwadkar, Optimizing Cs_2LiYCl_6 for fast neutron spectroscopy, Nuclear Instruments and Methods in Physics Research, Section A: Accelerators, Spectrometers, Detectors and Associated Equipment. 694 (2012) 140–146. https://doi.org/10.1016/j.nima.2012.07.021.

[9] D. Pérez-Loureiro, O. Kamaev, G. Bentoumi, L. Li, C. Jewett, M. Thompson, Evaluation of CLYC-6 and CLYC-7 scintillators for detection of nuclear materials, Nuclear Instruments and Methods in Physics Research, Section A: Accelerators, Spectrometers, Detectors and Associated Equipment. 1012 (2021) 165622. https://doi.org/10.1016/j.nima.2021.165622.

[10] A. Fazzi, M. Silari, Portable radiation detection device for operation in intense magnetic field. CERN/Polytechnic of Milan, joint patent. Patent Grant number 9977134 (13 July 2017).

[11] D. Celeste, A. Curioni, A. Fazzi, M. Silari, V. Varoli, B-RAD: A radiation survey meter for operation in intense magnetic fields, Journal of Instrumentation. 14 (2019). https://doi.org/10.1088/1748-0221/14/05/T05007.

[12] Products for nuclear safety, radiation detection and measurement - ELSE Nuclear. http://www.elsenuclear.com/it/ (accessed May 8, 2021).

[13] A. Giaz, N. Blasi, C. Boiano, S. Brambilla, F. Camera, C. Cattadori, S. Ceruti, F. Gramegna, T. Marchi, I. Mattei, A. Mentana, B. Million, L. Pellegri, M. Rebai, S. Riboldi, F. Salamida, M. Tardocchi, Fast neutron measurements with ^{7}Li and ^{6}Li enriched CLYC scintillators, Nuclear Instruments and Methods in Physics Research, Section A: Accelerators, Spectrometers, Detectors and Associated Equipment. 825 (2016) 51–61. https://doi.org/10.1016/j.nima.2016.03.090.

[14] J. Glodo, A. Gueorguiev, U. Shirwadkar, R. Hawrami, J. Tower, P. O'Dougherty, K.S. Shah, Integrated neutron detector for handheld systems, IEEE Transactions on Nuclear Science. 60 (2013) 903–907. https://doi.org/10.1109/TNS.2013.2252020.

[15] ENDF: Evaluated Nuclear Data File, (n.d.). https://www-nds.iaea.org/exfor/endf.htm (accessed June 7, 2021).

[16] CLYC Gamma-Neutron Scintillator for SPRDs and RIIDs | RMD, Dynasil, (n.d.). https://www.dynasil.com/product-category/scintillators/clyc-gamma-neutron-scintillators/ (accessed May 17, 2021).

500 [17] U. Bialkali, S. Bialkali, Photomultiplier Tube Series, (n.d.). www.hamamatsu.com (accessed
501 July 8, 2021).

502 [18] G. Van Rossum, F.L. Drake, Python 3 Reference Manual, CreateSpace, Scotts Valley, CA,
503 2009.

504 [19] G.F.Knoll, Radiation Detection and Measurements, 4th ed., 2010.

505 [20] K.A.A. Gamage, M.J. Joyce, N.P. Hawkes, A comparison of four different digital
506 algorithms for pulse-shape discrimination in fast scintillators, Nuclear Instruments and Methods in
507 Physics Research, Section A: Accelerators, Spectrometers, Detectors and Associated Equipment.
508 642 (2011) 78–83. https://doi.org/10.1016/j.nima.2011.03.065.

509 [21] MP 320 Neutron Generator, (n.d.).
510 https://www.thermofisher.com/order/catalog/product/1517021A#/1517021A (accessed June 1,
511 2021).

512 [22] F. Ferrulli, M. Silari, F. Thomsen, G. Zorloni, A thermal neutron source for the CERN
513 radiation Calibration Laboratory, Applied Radiation and Isotopes, 178 (2021) 109977.

514 [23] A. Mentana, F. Camera, A. Giaz, N. Blasi, S. Brambilla, S. Ceruti, L. Gini, F. Groppi, S.
515 Manenti, B. Million, S. Riboldi, Measurement of fast neutron detection efficiency with 6Li and 7Li
516 enriched CLYC scintillators, Journal of Physics: Conference Series. 763 (2016).
517 https://doi.org/10.1088/1742-6596/763/1/012006.

518 [24] N. Blasi, S. Brambilla, F. Camera, S. Ceruti, A. Giaz, L. Gini, F. Groppi, S. Manenti, A.
519 Mentana, B. Million, S. Riboldi, Fast neutron detection efficiency of 6Li and 7Li enriched CLYC
520 scintillators using an Am-Be source, Journal of Instrumentation. 13 (2018).
521 https://doi.org/10.1088/1748-0221/13/11/P11010.

522 [25] ISO - ISO 8529-1:2001 - Reference neutron radiations — Part 1: Characteristics and
523 methods of production, (n.d.). https://www.iso.org/standard/25666.html (accessed May 27, 2021).

524